strains, members of the Kim and Villeneuve labs for advice, many *C. elegans* researchers for use of their unpublished microarray data (supporting online material), A. Preble for comments on the manuscript, and K. Reddy for providing help with RNAi. Supported by an NIH genome training grant (J.M.S.), a Stanford Graduate Fellowship (E.S.), grants from the National Institute of General Medical Sciences and National Center for Research Resources (S.K.K.), and NSF grant ACI-0082554 under the Information Technology Research program (D.K.).

Supporting Online Material
www.sciencemag.org/cgi/content/full/1087447/DC1
Materials and Methods
SOM Text
Figs. S1 to S4
Tables S1 to S5

30 May 2003; accepted 13 August 2003
Published online 21 August 2003;
10.1126/science.1087447
Include this information when citing this paper.

Control Mechanism of the Circadian Clock for Timing of Cell Division in Vivo

Takuya Matsuo,[1,2]* Shun Yamaguchi,[1]* Shigeru Mitsui,[1] Aki Emi,[1] Fukuko Shimoda,[1] Hitoshi Okamura[1]†

Cell division in many mammalian tissues is associated with specific times of day, but just how the circadian clock controls this timing has not been clear. Here, we show in the regenerating liver (of mice) that the circadian clock controls the expression of cell cycle–related genes that in turn modulate the expression of active Cyclin B1-Cdc2 kinase, a key regulator of mitosis. Among these genes, expression of *wee1* was directly regulated by the molecular components of the circadian clockwork. In contrast, the circadian clockwork oscillated independently of the cell cycle in single cells. Thus, the intracellular circadian clockwork can control the cell-division cycle directly and unidirectionally in proliferating cells.

Circadian (~24-hour) rhythms and cell division are fundamental biological systems in most organisms. There is substantial evidence that, in mammals, circadian rhythms affect the timing of cell divisions in vivo. Day-night variations in both the mitotic index and DNA synthesis occur in many tissues (e.g., oral mucosa, tongue keratinocytes, intestinal epithelium, skin, and bone marrow) (*1*–*6*), some of which persist even in constant darkness (*7*). However, how the circadian clock controls the timing of cell divisions is not known.

To explore the relationship between cell division and circadian rhythms, we used a mouse model with partial hepatectomy (PH) (*8*–*13*). After a two-thirds partial hepatectomy (*14*), most of the remaining hepatocytes rapidly and simultaneously enter into the cell cycle, resulting in restoration of the liver mass in a few days.

Diurnal control of cell cycle in wild-type mice. PH was performed on mice (*15*) at ZT8 or ZT0 (ZT, Zeitgeber time in a 12 hour light–12 hour dark cycle; ZT0 represents lights on and ZT12, lights off) to compare the kinetics of subsequent cell cycles. The kinetics of S-phase (DNA-synthesizing) hepatocytes for both ZTs were comparable as determined by bromodeoxyuridine (BrdU) incorporation into nuclei, peaking at 36 hours after PH (Fig. 1A). In contrast, subsequent mitotic waves differed (Fig. 1B). When PH was performed at ZT8 (PH/ZT8), a massive entry of hepatocytes into the M phase occurred within 40 hours after PH. In the case of PH/ZT0, however, only a few cells entered the M phase within 44 hours, and a mitotic peak was reached 48 hours after PH. These results suggest that the time of operation has a marked effect on the timing of mitosis controlling the progression of cell cycling itself.

To investigate the molecular mechanism underlying this time of day–dependent regulation of the cell cycle, we examined the kinase activity of Cdc2 (*15*), an initiator of mitosis (*16*). Peaks of Cdc2 activity after PH/ZT8 and PH/ZT0 occurred 40 and 48 hours after PH, respectively, corresponding to the observed mitotic peaks (Fig. 1, B and C). This suggests that the regulation of the expression of the active Cdc2 kinase is an important process for the diurnal control of the cell cycle.

Analysis of the expression profiles of 68 cell cycle–related genes by DNA microarray and Northern blot analysis (fig. S1, A and B; fig. S2; and table S1) revealed that although 11 genes showed moderately different kinetics between PH/ZT8 and PH/ZT0 (differences of 1.5- to 2.2-fold or 0.67- to 0.42-fold; ratios of PH/ZT0 to PH/ZT8) (fig. S2 and table S2), only three genes—*cyclin B1*, *cdc2*, and *wee1*—showed remarkably different expression profiles (a difference of more than 2.7-fold) between 28 and 56 hours after PH (Fig. 1D).

The expression peaks of *cyclin B1* and *cdc2* transcripts, whose products form Cyclin B1-Cdc2-complex kinase, corresponded with Cdc2 kinase activity peaks (Fig. 1, C and D). Both mRNA peaks were delayed by 8 to 12 hours after PH/ZT0 as compared to PH/ZT8. The *wee1* gene product phosphorylates Cdc2 on Tyr-15 [p-Cdc2(Tyr 15)] and keeps it in an inactive form (*17*, *18*); the decrease of its mRNA corresponded with the increase of the Cdc2 kinase activity (Fig. 1, C and D) with the same time delay. These results suggest that the transcript-level regulation of *cyclin B1*, *cdc2*, and *wee1* contributes to the timing of entry into mitosis.

Impaired liver regeneration in arrhythmic *Cry*-deficient mice. Mice that lack the clock regulator *cryptochromes* (*Crys*) completely lack free-running rhythmicity. Yet, embryogenesis and postnatal development in these mice appear normal (*19*), suggesting that clock function is not absolutely required for cell cycling. Although the mean weights of the pre-PH livers of wild-type and *Cry*-deficient animals were the same ($P > 0.05$), the weights of the regenerating livers in *Cry*-deficient mice 72 hours after PH/ZT8 were significantly lower than those of wild-type mice (53.1 ± 3.0% and 64.1 ± 1.7% of pre-PH liver weight, respectively; Student's *t* test, $P < 0.05$) (Fig. 2A). This value for *Cry*-deficient mice was also lower than that of wild-type mice 72 hours after PH/ZT0 (66.4 ± 1.7%; $P < 0.01$), suggesting impairment of hepatocyte proliferation in *Cry*-deficient mice. However, in both genotypes, liver weight returned to pre-PH levels by day 10 (Fig. 2A), and histological analyses (including comparisons of the number and cell size of hepatocytes and average distances separating portal and central hepatic veins), did not reveal any major differences (*20*). This indicates that circadian clock function is required for efficient cell cycling in vivo.

The kinetics of S-phase hepatocytes after PH/ZT8 or PH/ZT0 in *Cry*-deficient and wild-type mice were comparable (Fig. 2B). However, in the subsequent mitotic wave, the maximum value of mitotic hepatocytes was low (less than 4% for both PH/ZT8 and PH/ZT0) (Fig. 2B). Furthermore, Cdc2 kinase activity was reduced (Figs. 2B and 1C). Therefore, the cell cycle progression from S to M phase was impaired during liver regeneration in *Cry*-deficient mice. In

[1]Division of Molecular Brain Science, Department of Brain Sciences, Kobe University Graduate School of Medicine, Chuo-ku, Kobe 650–0017, Japan. [2]Department of Physics, Informatics and Biology, Yamaguchi University, Yamaguchi 753–8512, Japan.

*These authors contributed equally to this work.
†To whom correspondence should be addressed. E-mail: okamurah@kobe-u.ac.jp

addition, because *Cry*-deficient mice did not exhibit a mitotic wave that depended on the time of operation, functional impairment of the control mechanism for mitotic timing in vivo is indicated.

To determine the molecular mechanism underlying the failure to progress through the cell cycle in *Cry*-deficient mice, we compared the expression profiles of the cell cycle–related genes between wild-type and *Cry*-deficient mice (fig. S1, C and D; fig. S3; and tables S1 and S3). After PH/ZT8, 7 of 68 analyzed genes showed different expression profiles: Differences of more than 2.7-fold or less than 0.37-fold (ratios of *Cry*-deficient to wild type) were observed between 32 and 56 hours after PH (Fig. 2C). These included the M-phase-related genes *cyclin B1*, *cdc2*, *wee1*, *Bub1*, and *p55CDC*; the S-phase- and M-phase-related gene *cyclin A2*; and the G1-phase-related gene *cyclin D1* (*21*). In *Cry*-deficient mice, the expression peaks of *cyclin B1*, *cdc2*, *Bub1*, *p55CDC*, and *cyclin A2* occurred 8 to 12 hours later than those in wild-type mice, corresponding to the peak mitotic timing (48 hours after PH) (Fig. 2, B and C). The expression profiles of *cyclin D1* and *wee1* transcripts were markedly different between *Cry*-deficient and wild-type mice throughout the liver regeneration process: *cyclin D1* expression decreased up to 86% and *wee1* expression increased up to 4.6-fold between 32 and 72 hours after PH (Fig. 2C). These results indicate that the expression of many cell cycle–related genes is deregulated in *Cry*-deficient mice and underlies impairment of cell-cycle progression.

Direct regulation of *wee1* transcription by circadian clockwork. The expression pattern of *wee1* during liver regeneration in *Cry*-deficient mice and its circadian cycling in normal mouse liver (*22*, *23*) raised the possibility that *wee1* transcription may be directly driven by the circadian oscillatory machinery. The expression level of WEE1 was reported to affect the timing of M phase entry in mammalian cells (*18*, *24*, *25*). In normal mouse livers, *wee1* mRNA displayed a robust circadian oscillation showing a 22.8-fold amplitude with a peak at circadian time (CT)8 (where CT0 is subjective dawn and CT12 is subjective dusk) (Fig. 3A). In *Cry*-deficient mice, *wee1* mRNA levels were high at both ZT0 and ZT12. However, in *Clock* mutant (*Clock/Clock*) mice (*26*), which carry dominant-negative *Clock* mutations (*27*), *wee1* expression was low at both ZTs (Fig. 3A). These expression profiles support the regulation of *wee1* transcription by circadian clock components: activated by CLOCK-BMAL1 heterodimers (*27*) and suppressed by PER/CRY proteins (*28*).

The CLOCK-BMAL1 complex acts on E-box (CACGTG) elements of target genes. Three E-box elements were found within 1.2 kb of the mouse *wee1* gene 5′-upstream region (Fig. 3B). CLOCK and BMAL1 together, but neither of them alone, produced a major increase in transcriptional activity through this fragment in transfected NIH3T3 cells (52.7-fold; Student's *t* test, $P < 0.001$) (Fig. 3C). This activation was reduced when all three E-boxes were mutated (82.6%; $P < 0.001$). PER1, PER2, and PER3 moderately reduced (32.1%, 71.8%, and 21.8%, respectively; $P < 0.05$), and CRY1 and CRY2 completely abolished the CLOCK-BMAL1-induced transcription. These results suggest that the *wee1* transcription is directly regulated by the core components of the feedback loop of the circadian oscillatory mechanism.

During liver regeneration, *wee1* mRNA levels in wild-type mice were high between ZT8 and ZT16 and low around ZT0 (Fig. 1D), similar to those of unoperated mice (Fig. 3A). In *Cry*-deficient mice, *wee1* mRNA levels were elevated throughout regeneration (Fig. 2C), whereas they were low in *Clock/Clock* mice (Fig. 3D). These results suggest that the direct regulation by the circadian clockwork is maintained even during the regeneration process.

Fluctuations in the quantities of *wee1* mRNA were also reflected in WEE1 protein and kinase activity levels in regenerating livers. In wild-type mice, the peaks of WEE1 protein expression occurred 36 hours after PH/ZT8 and 40 to 44 hours after PH/ZT0, 4 to 8 hours before the corresponding mitotic peaks (Fig. 3E) (*15*). Subsequently, the WEE1 protein levels rapidly decreased in both groups (Fig. 3E). These expression profiles were closely reflected by changes in

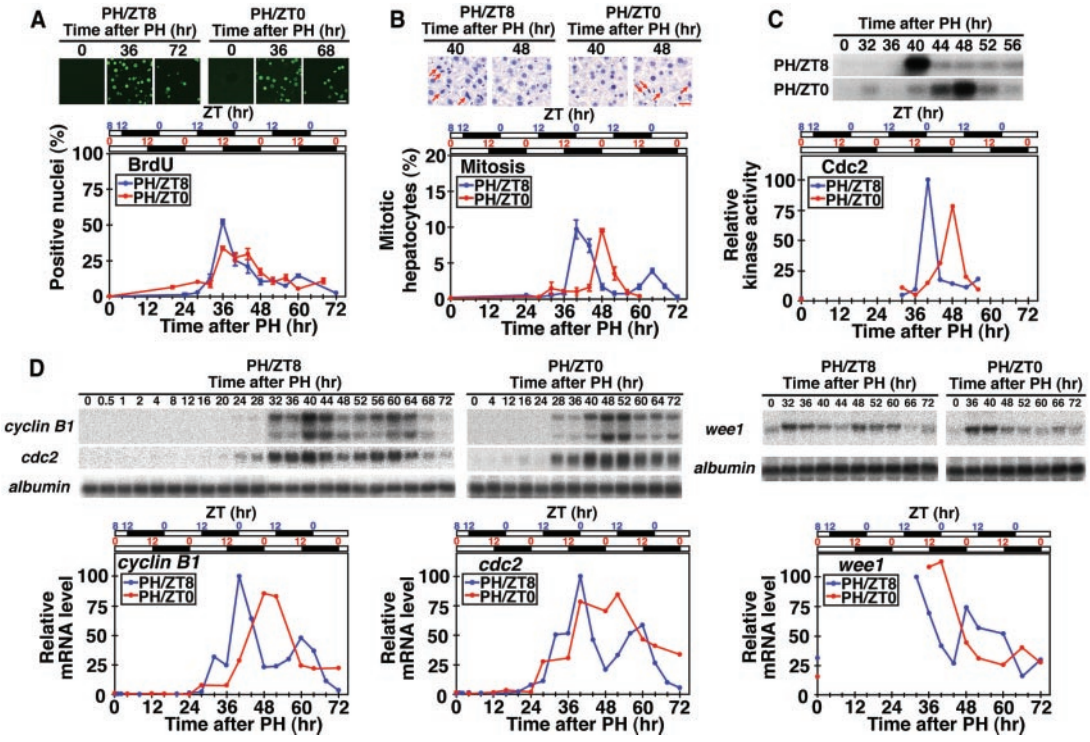

Fig. 1. Effects of time of PH on subsequent liver regeneration. White and black bars above the graphs represent times when lights were on or off, respectively. hr, hours. (**A**) Kinetics of DNA synthesis (BrdU-incorporation) in hepatocytes after PH/ZT8 and PH/ZT0. Values show mean percentage ± SEM in 2000 nuclei per animal. (**B**) Kinetics of mitotic hepatocytes after PH/ZT8 and PH/ZT0. Red arrows indicate mitotic nuclei. Values in the graph show mean percentage ± SEM in 3000 hepatocytes per animal. (**C**) Kinetics of Cdc2 kinase activity after PH/ZT8 and PH/ZT0. Cdc2 was immunoprecipitated from liver lysates and its kinase activity was determined by an in vitro kinase assay with histone H1 as the substrate. The peak value for the PH/ZT8 mice was adjusted to 100. (**D**) Temporal expression profiles of *cyclin B1*, *cdc2*, and *wee1* mRNAs after PH/ZT8 and PH/ZT0. Northern blot analyses for total RNAs (20 μg) isolated from the livers of operated mice are shown at the top. Quantified relative mRNA levels are shown in the graphs. The peak values for the PH/ZT8 mice were adjusted to 100. No variations were detected in the amounts of mRNA loaded as the result of hybridization with an *albumin* cDNA probe. Scale bars indicate 30 μm in (A) and (B).

the WEE1 kinase activity (Fig. 3F) (*15*). In *Cry*-deficient mice, WEE1 protein levels and WEE1 kinase activity were very high between 32 and 52 hours after PH (Fig. 3, E and F).

We next examined the kinetics of the phosphorylation of Cdc2 on Tyr-15, which is predominantly carried out by the WEE1 kinase (*17*, *18*). In wild-type mice, the p-Cdc2(Tyr 15) levels reached a peak 36 to 40 hours after PH/ZT8 and 44 to 48 hours after PH/ZT0 (Fig. 3G) (*15*). Thus, the peak expression for both ZTs was about 4 hours later than that of the corresponding WEE1 kinase activity. However, when the total amount of Cdc2 protein during liver regeneration was taken into account (Fig. 3G) and the ratios of p-Cdc2(Tyr 15) to Cdc2 were calculated, the peak times for both ZTs corresponded well with the WEE1 kinase activity peaks (Fig. 3, F and G). These peaks occurred 4 hours before the corresponding Cdc2 kinase activity peaks (Fig. 1C). In *Cry*-deficient mice, both the amount of p-Cdc2(Tyr 15) and the p-Cdc2(Tyr 15)/Cdc2 ratios were high between 32 and 52 hours after PH (Fig. 3G). This, at least in part, accounts for the low activity of the Cdc2 kinase in *Cry*-deficient mice (Fig. 2B). The increase in p-Cdc2(Tyr 15) is thought to be due to the high level of WEE1 kinase expression, because Myt1, another Cdc2(Tyr 15)-phosphorylating kinase (*29*), showed no significant difference in the quantities of mRNA and protein between wild-type and *Cry*-deficient mice (fig. S4). Taken together, the data suggest that the fluctuations in the quantity of *wee1* mRNA are closely reflected by its protein and kinase activity, target phosphorylation, and Cdc2 kinase activity. Thus, the circadian clock–*wee1* pathway can control the cell cycle in vivo.

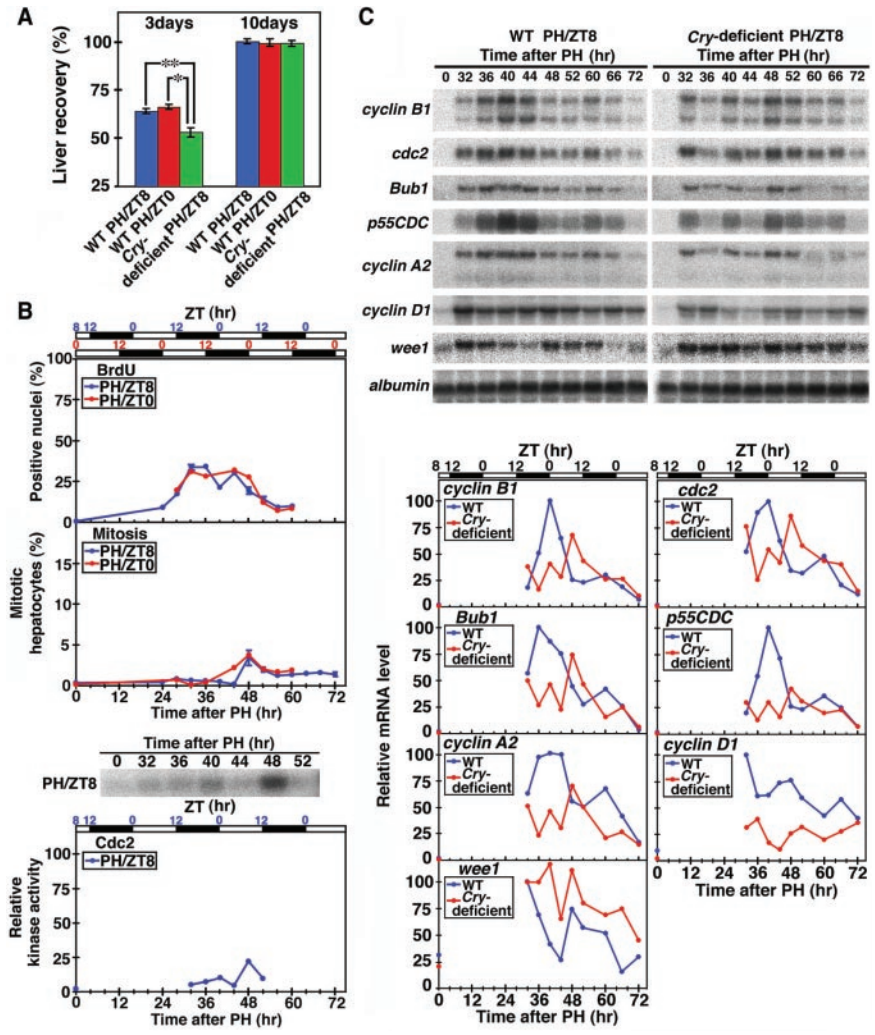

Fig. 2. Liver regeneration in *Cry*-deficient mice. (**A**) Liver weights of wild-type (WT; PH/ZT8 and PH/ZT0) and *Cry*-deficient (PH/ZT8) mice 72 hours and 10 days after PH. Pre-PH liver weight (removed liver weight × 1/0.67) of the animals was adjusted to 100%. Values represent the mean ± SEM (n = 4 to 6). Single and double asterisks denote statistically significant differences ($P < 0.01$ and $P < 0.05$, respectively). (**B**) Kinetics of BrdU-stained hepatocytes (top), mitosis (middle), and Cdc2 kinase activity (bottom) in *Cry*-deficient mice after PH. Values in the top and middle graphs were determined as in Fig. 1, A and B. In the bottom graph, relative values were calculated by setting the peak value for PH/ZT8 in Fig. 1C as 100. (**C**) Temporal expression profiles of the cell cycle-related genes that showed markedly different expression patterns between wild-type and *Cry*-deficient mice after PH. Northern blot analyses for the regenerating livers after PH/ZT8 are shown as in Fig. 1D. The peak values for the wild-type mice were adjusted to 100.

Functional clock in dividing hepatocytes. To determine whether the circadian clock continues to function during the massive entry of hepatocytes into the cell cycle, we examined expression profiles of clock components *Per1*, *Per2*, *Cry1*, and *Bmal1*. Robust oscillations in these mRNAs with a periodicity of 24 hours (fig. S5, A and B) were observed in unoperated wild-type mice. After PH/ZT8 or PH/ZT0, these expression profiles were mostly conserved, even on the first day after PH (fig. S5, A and B). At the same time, more than 70% of hepatocytes (71.0 ± 6.2% for PH/ZT8 and 70.1 ± 0.7% for PH/ZT0) were involved in cell cycling on the second day (fig. S5C). These results suggest that the intrinsic circadian clock continued to function in the regenerating liver even when the majority of the hepatocytes were going through the cell cycle.

At the single-cell level, PER2 protein expression in hepatocyte nuclei, as determined by immunohistochemistry (*15*), was observed in the livers of unoperated wild-type mice at ZT20, 4 hours after the *Per2* mRNA peaks (Fig. 4A). No cytoplasmic or nuclear PER2 was found between ZT0 and ZT16. PER2 immunoreactivity in nonparenchymal cells, including endothelial, Kupffer, and ductal cells, was below the level of detection at all times (*20*). After PH/ZT8, nuclear PER2 was found again at exactly ZT20 (12, 36, and 60 hours after PH) (Fig. 4B). Moreover, PER2 accumulated in nuclei of BrdU-stained cells, exactly as in unstained cells (Fig. 4B). This was also observed after PH/ZT0 (fig. S6). Therefore, the circadian clockwork oscillated accurately in a single proliferating cell. Furthermore, the circadian output genes *dbp*, *hlf*, *tef*, *e4bp4*, and *cyp7a* displayed robust oscillations in their transcript expression levels throughout the regeneration process (fig. S7), indicating that the intracellular circadian clockwork is functional and is able to control the timing of the cell cycle–related gene expression during the regenerating process.

Finally, we investigated whether the circadian rhythms of the clock gene expression persist in proliferating hepatocytes in the absence of cell cycling. Before partial hepatectomy performed at ZT8, the mice were given retrorsine (*15*), which inhibits hepatocyte cell division for several weeks (*30*). This treatment resulted in a cell cycle block that allowed DNA synthesis but almost completely eliminated the subsequent mitotic division (the highest value of the mitotic index between 36 to 64 hours after PH was less than 0.2%) (fig. S8A).

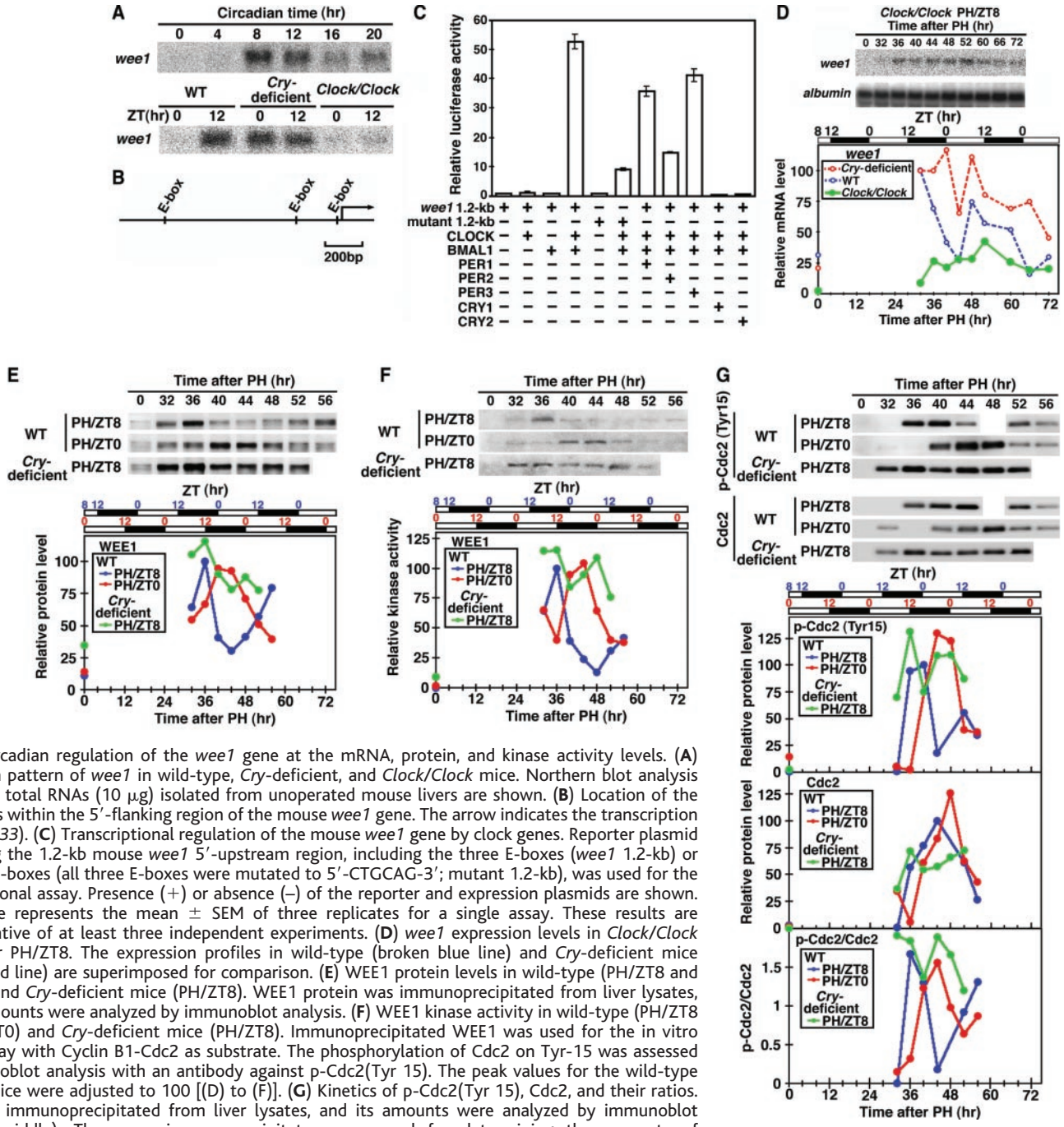

Fig. 3. Circadian regulation of the *wee1* gene at the mRNA, protein, and kinase activity levels. (**A**) Expression pattern of *wee1* in wild-type, *Cry*-deficient, and *Clock/Clock* mice. Northern blot analysis results for total RNAs (10 μg) isolated from unoperated mouse livers are shown. (**B**) Location of the E-box sites within the 5′-flanking region of the mouse *wee1* gene. The arrow indicates the transcription start site (*33*). (**C**) Transcriptional regulation of the mouse *wee1* gene by clock genes. Reporter plasmid containing the 1.2-kb mouse *wee1* 5′-upstream region, including the three E-boxes (*wee1* 1.2-kb) or mutated E-boxes (all three E-boxes were mutated to 5′-CTGCAG-3′; mutant 1.2-kb), was used for the transcriptional assay. Presence (+) or absence (–) of the reporter and expression plasmids are shown. Each value represents the mean ± SEM of three replicates for a single assay. These results are representative of at least three independent experiments. (**D**) *wee1* expression levels in *Clock/Clock* mice after PH/ZT8. The expression profiles in wild-type (broken blue line) and *Cry*-deficient mice (broken red line) are superimposed for comparison. (**E**) WEE1 protein levels in wild-type (PH/ZT8 and PH/ZT0) and *Cry*-deficient mice (PH/ZT8). WEE1 protein was immunoprecipitated from liver lysates, and its amounts were analyzed by immunoblot analysis. (**F**) WEE1 kinase activity in wild-type (PH/ZT8 and PH/ZT0) and *Cry*-deficient mice (PH/ZT8). Immunoprecipitated WEE1 was used for the in vitro kinase assay with Cyclin B1-Cdc2 as substrate. The phosphorylation of Cdc2 on Tyr-15 was assessed by immunoblot analysis with an antibody against p-Cdc2(Tyr 15). The peak values for the wild-type PH/ZT8 mice were adjusted to 100 [(D) to (F)]. (**G**) Kinetics of p-Cdc2(Tyr 15), Cdc2, and their ratios. Cdc2 was immunoprecipitated from liver lysates, and its amounts were analyzed by immunoblot analysis (middle). The same immunoprecipitates were used for determining the amounts of p-Cdc2(Tyr 15) by immunoblot analysis with the antibody against p-Cdc2(Tyr 15) (top). The peak values for the wild-type PH/ZT8 mice were adjusted to 100 (top and middle). Each value in the top graph was simply divided by the corresponding middle graph value (bottom).

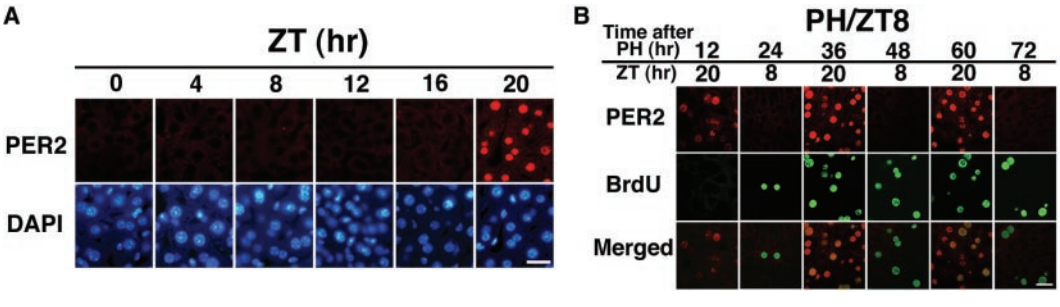

Fig. 4. PER2 protein expression in proliferating hepatocytes. (**A**) Immunofluorescence analysis (red) showing the temporal expression profile of PER2 protein in unoperated control livers. Nuclei were counterstained with 4′,6-diamidino-2-phenylindole (blue). (**B**) Nuclear PER2 accumulation (red) in BrdU-stained (green) and unstained hepatocytes at regular time intervals after PH/ZT8. Scale bars, 30 μm.

Even under these conditions, PER2 expression was still observed in almost all hepatocytes (99.1% of 2000 cells) at exactly ZT20 (36 and 60 hours after PH) (fig. S8B), indicating that the circadian oscillatory mechanism in proliferating hepatocytes did not require the help of a cell cycle for its normal functioning.

Conclusion and perspective. We have observed that the circadian clockwork can oscillate accurately and independently of the cell cycle in proliferating hepatocytes and that this intrinsic oscillatory mechanism may participate in regulating the timing and efficiency of cell-cycle events through clock-controlled genes such as *wee1*. Although external humoral and/or neural timing cues may also participate in cell-cycle regulation (*12*), the presence of intracellular pathways from the circadian clockwork to the cell-cycle system indicates a strong correlation of the timing of clock gene expression with the timing of cell-cycle events in not only regenerating liver but also continuously proliferating tissues (e.g., oral and gastrointestinal mucosa, skin, and bone marrow). Although only a few studies have examined both clock gene expression and cell-cycle events simultaneously in proliferating tissues (*31*), the following relationship may be conserved: Expression of *wee1* is high when the transcript of *Per1*, another CLOCK-BMAL1-driven gene, is abundant in these tissues, and the entry into the M phase is suppressed during that time of day. The findings may extend to understanding the circadian phase–dependent toxicity and antitumor effects of several chemotherapy drugs (*32*).

References and Notes

1. G. A. Bjarnason, R. Jordan, *Prog. Cell Cycle Res.* **4**, 193 (2000).
2. M. N. Garcia, C. G. Barbeito, L. A. Andrini, A. F. Badran, *Cell Biol. Int.* **25**, 179 (2001).
3. L. E. Scheving, T. H. Tsai, L. A. Scheving, *Am. J. Anat.* **168**, 433 (1983).
4. K. N. Buchi, J. G. Moore, W. J. Hrushesky, R. B. Sothern, N. H. Rubin, *Gastroenterology* **101**, 410 (1991).
5. W. R. Brown, *J. Investig. Dermatol.* **97**, 273 (1991).
6. R. Smaaland, *Prog. Cell Cycle Res.* **2**, 241 (1996).
7. L. E. Scheving, J. E. Pauly, H. von Mayersbach, J. D. Dunn, *Acta Anat.* **88**, 411 (1974).
8. J. J. Jaffe, *Anat. Rec.* **120**, 935 (1954).
9. C. P. Barnum, C. D. Jardetsky, F. Halberg, *Tex. Rep. Biol. Med.* **15**, 134 (1957).
10. E.G. Bade, I. L. Sadnik, C. Pilgrim, W. Maurer, *Exp. Cell Res.* **44**, 676 (1966).
11. M. Souto, J. M. Llanos, *Chronobiol. Int.* **2**, 169 (1985).
12. H. Barbason *et al.*, *In Vivo* **9**, 539 (1995).
13. B. Barbiroli, V. R. Potter, *Science* **172**, 738 (1971).
14. G. M. Higgins, R. M. Anderson, *Arch. Pathol.* **12**, 186 (1931).
15. Materials and methods are available as supporting material on *Science* Online.
16. R. Ohi, K. L. Gould, *Curr. Opin. Cell Biol.* **11**, 267 (1999).
17. L. L. Parker, H. Piwnica-Worms, *Science* **257**, 1955 (1992).
18. C. H. McGowan, P. Russell, *EMBO J.* **12**, 75 (1993).
19. G. T. J. van der Horst *et al.*, *Nature* **398**, 627 (1999).
20. T. Matsuo, unpublished data.
21. J. Pines, *Nature Cell Biol.* **1**, E73 (1999).
22. R. A. Akhtar *et al.*, *Curr. Biol.* **12**, 540 (2002).
23. K. F. Storch *et al.*, *Nature* **417**, 78 (2002).
24. C. J. Rothblum-Oviatt, C. E. Ryan, H. Piwnica-Worms, *Cell Growth Differ.* **12**, 581 (2001).
25. R. Heald, M. McLoughlin, F. McKeon, *Cell* **74**, 463 (1993).
26. D. P. King *et al.*, *Cell* **89**, 641 (1997).
27. N. Gekakis *et al.*, *Science* **280**, 1564 (1998).
28. K. Kume *et al.*, *Cell* **98**, 193 (1999).
29. F. Liu, J. J. Stanton, Z. Wu, H. Piwnica-Worms, *Mol. Cell. Biol.* **17**, 571 (1997).
30. S. Laconi *et al.*, *J. Hepatol.* **31**, 1069 (1999).
31. G. A. Bjarnason *et al.*, *Am. J. Pathol.* **158**, 1793 (2001).
32. F. Levi, *Chronobiol. Int.* **19**, 1 (2002).
33. H. Kawasaki *et al.*, *EMBO J.* **20**, 4618 (2001).

34. The authors wish to thank M. Iwai (Kyoto Prefectural University of Medicine) for advising the technique of hepatectomy, G. T. J. van der Horst (Erasmus University) for providing access to *Cry*-deficient mice, and A. Ishida and T. Okamoto (Kobe University) for technical assistance. Supported in part by grants from the Special Coordination Funds; the Grant-in-Aid for the Scientific Research on Priority Areas of the Ministry of Education, Culture, Sports, Science, and Technology of Japan; the Kanae Foundation for Life and Sociomedical Science; and the Inamori Foundation.

Supporting Online Material

www.sciencemag.org/cgi/content/full/1086271/DC1
Materials and Methods
Figs. S1 to S8
Tables S1 to S3
References

3 August 2003; accepted 8 August 2003
Published online 21 August 2003;
10.1126/science.1086271
Include this information when citing this paper.

REPORTS

Phosphadioxirane: A Peroxide from an Ortho-Substituted Arylphosphine and Singlet Dioxygen

David G. Ho,* Ruomei Gao,* Jeff Celaje, Ha-Yong Chung, Matthias Selke†

We prepared the primary adduct for the reaction of singlet dioxygen ($^1O_2$) with an arylphosphine by using the sterically hindered arylphosphine tris(*o*-methoxyphenyl)phosphine. The resulting phosphadioxirane has a dioxygen molecule triangularly bound to the phosphorus atom. Olefin trapping experiments show that the phosphadioxirane can undergo nonradical oxygen atom–transfer reactions. Under protic conditions, two different intermediates are formed during the reaction of singlet dioxygen with tris(*o*-methoxyphenyl)phosphine, namely, the corresponding hydroperoxy arylphosphine and a hydroxy phosphorane. Experiments with other arylphosphines possessing different electronic and steric properties demonstrate that the relative stability of the tris(*o*-methoxyphenyl)phosphadioxirane is due to both steric and electronic effects.

The reactions of singlet dioxygen ($^1O_2$) with organic sulfides (*1–4*) and phosphines (*5–8*) represent rare examples of nonradical aerobic oxidations, and the mechanisms of these deceptively simple processes have proven to be very complicated. Whereas spin-forbidden oxidation reactions involving ground-state dioxygen ($^3O_2$) have large kinetic barriers, reactions involving singlet dioxygen ($^1O_2$) often have enthalpies of activation near zero and can consequently be carried out at very low temperatures. Nevertheless, despite numerous efforts, peroxidic intermediates have not been directly observed during the reactions of $^1O_2$ with organic sulfides and phosphines, largely because such intermediates should be even better oxidants than $^1O_2$ itself. However, such intermediates may also represent synthetic "oxene-like" oxidants derived from molecular oxygen that could be used for the oxidation of organic molecules by nonradical pathways. We have recently reported an unusual intramolecular oxidation pathway during the photooxidation of tris(*ortho*-methoxyphenyl)phosphine (**1**) and have shown that there exists a phosphine cone-angle dependence for this reactive channel of the putative peroxidic intermediate (*8*). The bulky ortho substituents shield the phosphorus atom somewhat from intermolecular attack by a second phosphine, leading to the observed intramolecular reactivity. We have also noted that physical quenching of singlet oxygen by **1** at room temperature is insignificant (*8*) (Fig. 1).

Department of Chemistry and Biochemistry, California State University, Los Angeles, Los Angeles, CA 90032, USA.

*These authors contributed equally to this work.
†To whom correspondence should be addressed. E-mail: mselke@calstatela.edu